Advancement of Reference-free Diagnosis for Aging Aircraft Monitoring

Hoon Sohn, Ph.D.

Associate Professor

Civil and Environmental Engineering Department

Korea Advanced Institute of Science and Technology

Funding Agency: Asian Office of Aerospace Research and Development, Department of the Air Force, US

Funding Period: July 01, 2009 to June 30, 2010

Funding level: $25,000 for one year

1. Project Summary

The goal of this project is to develop a new NDT technique/algorithm based on Lamb waves, in which damage can be detected "without relying on past reference data." In particular, a NDT methodology will be formulated for detecting defects such as crack, corrosion and delamination commonly found in aircraft. The proposed concept of "reference-free" damage diagnosis attempts to address some of the fundamental technical hurdles that have to be overcome before NDT systems can be deployed for continuous monitoring of aircraft. The intent of the present approach is not to disregard useful prior knowledge or information gained but to relax explicit dependency on baseline data so that the proposed methodology can be made more attractive for aircraft monitoring during its normal operation. By incorporating the proposed approach to the conventional NDT techniques, it is envisioned that more reliable damage diagnosis can be achieved. New reference-free damage diagnosis techniques developed in this study are:

- **Reference-free crack detection using transducer impedance:** A new concept of reference-free damage detection methodology is developed using transfer impedances to detect crack damage in a plate-like structure without using previously collected baseline data. This technique compares estimated the energy content of crack-induced mode conversion to the background noise energy level. The transfer impedance technique advances the previously developed time-domain technique by detecting not only a single crack but also multiple cracks.
- **Instantaneous crack detection under varying temperature and static loading conditions:** An improved reference-free crack detection technique is developed using a newly designed PZT transducer. The major advancement of the proposed technique are (1) single surface installation of PZT transducers to overcome limited access to both surfaces of some structural systems like aircraft and pipelines (2) detection of cracks even when measured Lamb wave time signals are complex due to existence of multiple modes and reflections.

2. Project Activities

A. Reference-free crack detection using transducer impedance

A.1. Introduction

Conventional impedance-based damage detection techniques have been shown to be vulnerable to other types of changes such as temperature variation that may not be relevant to defects of interest. One of potential disadvantages of the conventional techniques is frequent false-alarms due to these undesirable variations that may occur particularly for field applications. In order to reduce these false-alarms, a new methodology that utilizes transfer impedances obtained between two pairs of collocated PZT patches instead of the electromechanical impedance obtained at one PZT patch is proposed in this study. The proposed technique seeks Lamb mode conversion effects caused by the presence of crack damage in plate structures. Furthermore, an instantaneous damage classification is carried out by

Report Documentation Page

Form Approved
OMB No. 0704-0188

1. REPORT DATE	2. REPORT TYPE	3. DATES COVERED
29 SEP 2010	**Final**	**01-07-2009 to 01-06-2010**

4. TITLE AND SUBTITLE
Advancement of Reference-free Diagnosis for Aging Aircraft Monitoring

5a. CONTRACT NUMBER
FA23860914125

5b. GRANT NUMBER

5c. PROGRAM ELEMENT NUMBER

6. AUTHOR(S)
Hoon Sohn

5d. PROJECT NUMBER

5e. TASK NUMBER

5f. WORK UNIT NUMBER

7. PERFORMING ORGANIZATION NAME(S) AND ADDRESS(ES)
Korean Advanced Institute of Science and Technology,373-1 Guseong-Dong,Daejeon 305-01,Korea (South),NA,NA

8. PERFORMING ORGANIZATION REPORT NUMBER
N/A

9. SPONSORING/MONITORING AGENCY NAME(S) AND ADDRESS(ES)
AOARD, UNIT 45002, APO, AP, 96337-5002

10. SPONSOR/MONITOR'S ACRONYM(S)
AOARD

11. SPONSOR/MONITOR'S REPORT NUMBER(S)
AOARD-094125

12. DISTRIBUTION/AVAILABILITY STATEMENT
Approved for public release; distribution unlimited

13. SUPPLEMENTARY NOTES

14. ABSTRACT

The goal of this project was to develop a new NDT technique/algorithm based on Lamb waves, in which damage can be detected ?without relying on past reference data.? In particular, a NDT methodology was formulated for detecting defects such as crack, corrosion and delamination commonly found in aircraft. The proposed concept of ?reference-free? damage diagnosis attempts to address some of the fundamental technical hurdles that have to be overcome before NDT systems can be deployed for continuous monitoring of aircraft. The intent of the present approach is not to disregard useful prior knowledge or information gained but to relax explicit dependency on baseline data so that the proposed methodology can be made more attractive for aircraft monitoring during its normal operation. By incorporating the proposed approach to the conventional NDT techniques, it is envisioned that more reliable damage diagnosis can be achieved. New reference-free damage diagnosis techniques developed in this study are &#56256;&#56451; Reference-free crack detection using transducer impedance: and &#56256;&#56451; Instantaneous crack detection under varying temperature and static loading conditions

15. SUBJECT TERMS
Aging Aircraft, Non-destructive Evaluation

16. SECURITY CLASSIFICATION OF:			17. LIMITATION OF ABSTRACT	18. NUMBER OF PAGES	19a. NAME OF RESPONSIBLE PERSON
a. REPORT	b. ABSTRACT	c. THIS PAGE			
unclassified	**unclassified**	**unclassified**	**Same as Report (SAR)**	**16**	

comparing mode conversion energy among several combinations of measured signals without any user-specified threshold or relying on the baseline data.

A.2. Transfer impedance-based reference-free technique

A.2.1. PZT poling characteristic-based crack-induced mode conversion extraction

PZT materials have been widely utilized for exciting and measuring guided Lamb wave propagations for SHM applications. If Lamb waves propagating along a thin plate with a uniform thickness encounter a discontinuity such as a sudden thickness change of the plate, some portion of the waves are reflected at the discontinuity point and others are transmitted through it. When a S_0 mode arrives at the discontinuity, the transmitted wave is separated into S_0 and A_0 modes (denoted as S_0/S_0 and A_0/S_0, respectively). In a similar manner, an A_0 mode is also divided into S_0 and A_0 modes (S_0/A_0 and A_0/A_0). Furthermore, the reflected waves at the discontinuity are also converted and split into S_0 and A_0 modes. This phenomenon is called mode conversion. The phase of guided Lamb wave modes depends on (1) the poling direction of exciting and sensing PZT patches and (2) whether a PZT patch is attached either on the top or on the bottom surface of a plate. By using the PZT polarization characteristic, the mode conversion due to crack formation can be extracted without using any prior baseline data.

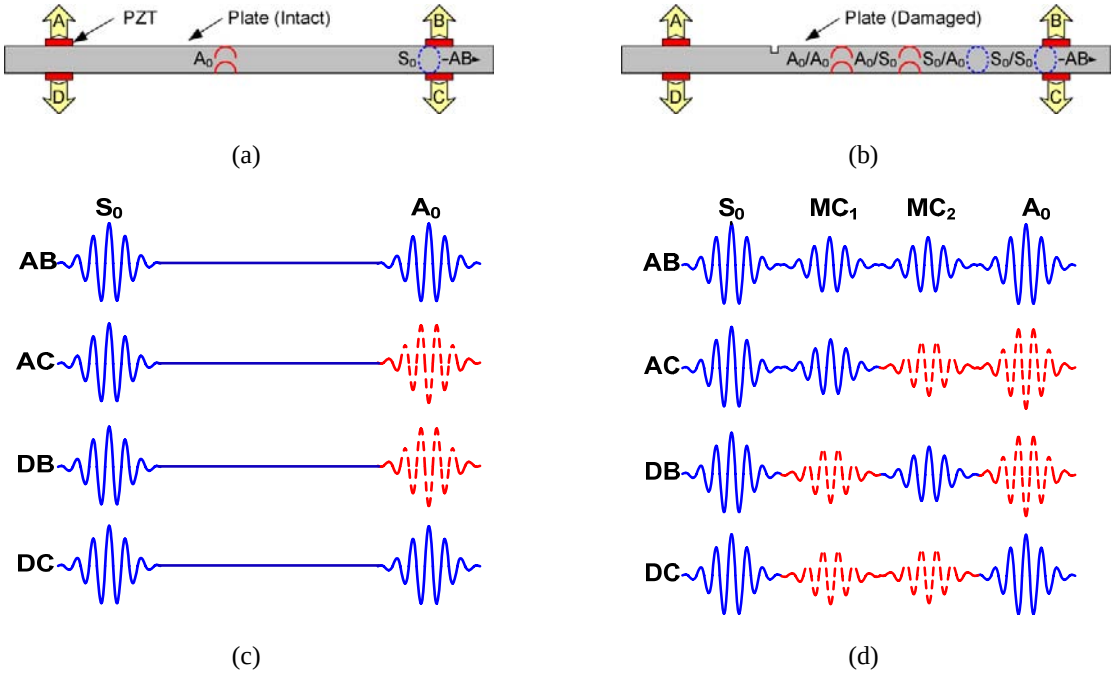

FIG. 1. Comparison of signals obtained from the undamaged and damaged conditions: (a) intact case (without a notch), (b) damaged case (with a notch), (c) signals without a notch, and (d) signals with a notch.

Author's research group has shown that the relative phases among measured Lamb wave modes change according to (1) the side of the PZT patch placement (top or bottom surface), (2) the PZT poling direction and (3) the deformed shape of Lamb waves (symmetric or anti-symmetric) as displayed in Fig. 1. Herein, it is assumed that a narrowband tone-burst signal is applied as an input, and a driving frequency is chosen such that only the fundamental symmetric (S_0) and asymmetric (A_0) modes are generated. Figs 1(a) and 1(c) present the relative phase information among Lamb wave modes measured from an intact case while Figs 1(b) and 1(d) illustrate a damaged case with a notch. It is noted that the signs of the fundamental (non-converted) modes (S_0 and A_0) are not affected by crack formation. On the other hand, the signs of newly generated (converted) modes (A_0/S_0 and S_0/A_0) are altered depending on the characteristics of a discontinuity that the launching Lamb mode is passing through. When the plate is in a pristine condition, it is observed that signal AB (or AC) becomes identical to signal DC (or DB), as shown in Fig. 1(c). When a crack is formed between PZTs A and B (or PZTs D and C) as shown in Fig. 1(d), signal AB (or

AC) is no longer identical to signal DC (or DB) due to different phases among the converted modes. In Fig. 1(d), the first and second arrivals of the converted modes are defined as MC_1 and MC_2, respectively. Note that MC_1 and MC_2 could be either S_0/A_0 or A_0/S_0 modes depending on the relative position of the crack with respect to the actuating and sensing PZTs. For instance, MC_1 in signal AB becomes a S_0/A_0 mode when the notch is closer to PZT A than PZT B. This is because the S_0/A_0 mode arrives at PZT B earlier than the A_0/S_0 mode. Similarly, MC_2 in signal AB represents the A_0/S_0 mode. Here, the signs of the MC_1 and MC_2 modes in signal AB are assumed to be positive so that the relative phases of the MC_1 and MC_2 modes in other signals (signals AC, DB and DC) can be compared with. For instance, it is shown in Fig. 1 (d) that the MC_1 and MC_2 modes in signal DC are out of phase when compared with the converted modes in signal AB. On the other hand, the S_0 and A_0 modes in signal DC are identical to the corresponding fundamental modes in signal AB. Therefore, the mode conversions (MC_1 and MC_2 modes) can be extracted simply by subtracting signal DC and from signal AB (see the Fig. 2(a)). Similarly, the converted modes can be isolated by subtracting signal DB from signal AC (see the Fig. 2(b)). Based on these observations, it can be concluded that additional converted modes (MC_1 and MC_2) generated by a notch can be simply extracted by subtracting signal DC from signal AB (or by subtracting signal DB from signal AC). Here, the difference is that the MC_1 and MC_2 modes are in phase in Fig. 2(a) while they are out of phase in Fig. 2(b).

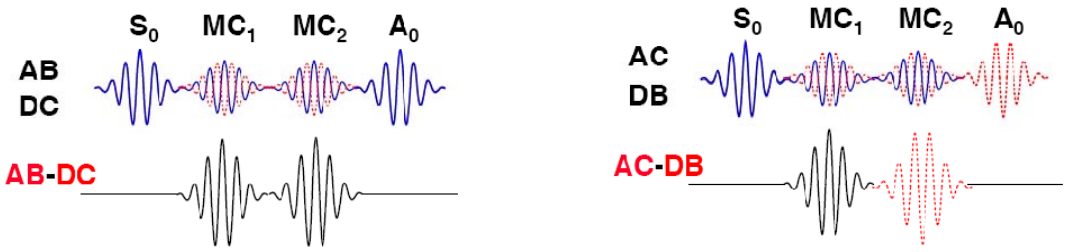

(a) (b)

FIG. 2. Extraction of crack-induced mode conversions by subtracting measured time signals: (a) mode conversions obtained by subtracting signal DC from signal AB and (b) mode conversions obtained by subtracting signal DB from signal AC.

A.3. Transfer impedance-based reference-free technique

A.3.1. Composition of mode conversion signals from measured time signals

The mode conversions (MC_1 and MC_2) generated by a notch can be easily extracted by (1) subtracting signal DC from signal AB or (2) subtracting signal DB from signal AC. Note that the MC_1 modes in signals (AB-DC) and (AC-DB) are in-phase, while the MC_2 modes are fully out-of-phase. Then, MC_1 and MC_2 modes can be further isolated from signals (AB-DC) and (AC-DB) through their summation or subtraction. Finally, four kinds of composed signals (M1, M2, M3 and M4) can be defined as follows: (1) Signal M1 given by $(AB - DC) / 2$: contains MC_1 and MC_2; (2) Signal M2 given by $(AC - DB) / 2$: contains MC_1 and MC_2; (3) Signal M3 given by $\{(AB\text{-}DC) + (AC\text{-}DB)\} / 4$: contains only MC_1; and (4) Signal M4 given by $\{(AB\text{-}DC) - (AC\text{-}DB)\} / 4$: contains only MC_2. Note that signals M1-M4 are normalized so that MC_1 and MC_2 modes in all composed signals have the same amplitude. These composed signals can be classified into Class A that contains both mode conversions (MC_1 and MC_2) and Class B that includes only one mode conversion (MC_1 or MC_2): The first two (M1 and M2) and the last two (M3 and M4) belong to Classes A and B, respectively, as displayed in Fig. 3. In Fig. 3, the compositions of signals M1-M4 are illustrated assuming that there are only two mode conversions (MC_1 and MC_2) for simplicity. In reality, these compositions can be generalized even when there are multiple mode conversions. The existence of multiple mode conversions occurs (1) when a long time signal with reflections of these converted modes from boundaries is considered and (2) when higher modes are excited at a certain driving frequency. Regardless of the existence of multiple mode conversions, the converted modes can be divided into two categories: Ones converted from symmetric modes to anti-symmetric modes and the others transformed from anti-symmetric modes to

symmetric modes. They are always generated in pairs. Once we denote these two types of mode conversions as MC_1 and MC_2, the rest of the composition operations can proceed as before.

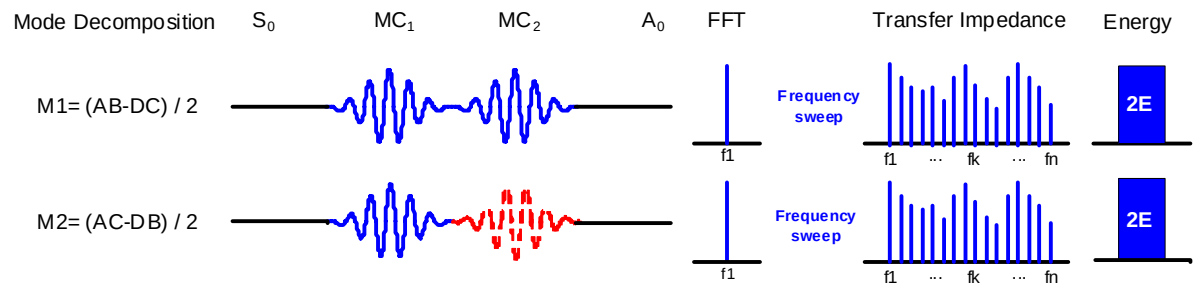

(a)

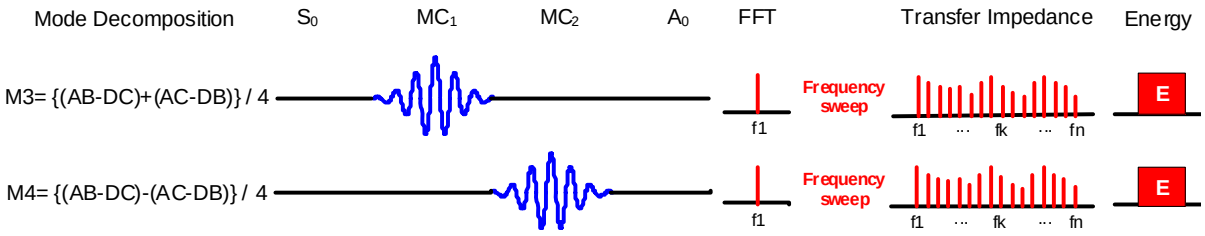

(b)

FIG. 3. Transfer impedances of composed mode conversion signals M1-M4: (a) Class A: contains both mode conversions (MC_1 and MC_2) and (b) Class B: contains only one mode conversion (MC_1 or MC_2) (it can be shown that the average energy levels of Class A transfer impedances (for M1 and M2) are approximately twice of these of Class B transfer impedances (for M3 and M4)).

A.3.2. Calculation of transfer impedances of composed signals M1, M2 M3 and M4

In this subsection, the transfer-impedances are calculated from the composed signals (M1-M4). Here, a transfer impedance is defined as a frequency-response-function between a pair of PZT patches (one for 'input' and the other for 'output') while the driving frequency is swept. To evaluate the level of the mode conversions produced by a crack, the energy contents of the composed signals M1-M4 averaged over a certain frequency band have been computed. First, Fast Fourier Transform (FFT) of the composed signals (M1-M4) is computed at a given driving frequency. Then, the same procedure is repeated over a specified frequency band to obtain transfer impedances. Finally, the total energy of each signal is computed by summing the magnitudes of its transfer impedance over the entire frequency range investigated. Fig. 3 presents that the transfer impedances of the composed signals have a specific energy-ratio of "2:1" between Class A and Class B signals in a damaged condition. However, it should be noted that the energy ratio will not be always perfectly 2 to 1. For instance, the MC_1 and MC_2 modes in signal M2 can be fully overlapped and then the corresponding energy can be zero. On the other hand, it is expected that when there exist only initial errors (no mode conversions) in a healthy condition, the energy ratio between Classes A and becomes arbitrary.

A.3.3. Development of an instantaneous damage classifier

Based on the findings above, a damage classifier that operates on transfer impedance energy is developed in this study. The objective here is to determine the existence of damage (or mode conversion) solely based on the signals measured from the current state of the structure. Often damage classification requires establishment of a threshold value (for unsupervised learning) or a decision boundary (for supervised learning) based on previously obtained baseline data or training data set. However, it has been shown that such dependences on the baseline data can produce frequent false alarms of damage. As mentioned previously, the energy ratio between the transfer impedances in

Classes A and B would not be exactly 2 to 1. However, it is expected that the transfer impedance energy of signals M1 and M2 in Class A be certainly larger than those of signals M3 and M4 in Class B in the presence of mode conversion. Based on this observation, the following damage classification statement can be established:

"If the minimum of out-of-class energy differences is larger than the maximum of within-class energy differences, a crack exists. Otherwise, there is no crack".

The minimum of out-of-class energy differences and the maximum of within-class energy differences are defined as |min(X1, X2)-max(X3, X4)| and max(|X1-X2|, |X3-X4|), respectively. Here, X1, X2, X3 and X4 denote the mean values of the transfer impedance energy computed for signals M1-M4 over the inspected frequency band, respectively. The maximum of within-class energy differences represents the maximum level of the initial errors, and the minimum of out-of-class energy differences denotes the minimum level of the energy increase due to crack-induced mode conversion. That is, this damage classifier identifies crack formation if the crack-induced mode conversion produces mode conversion energy larger than energy variation due to the initial errors.

A.4. Experimental study

To verify the effectiveness of the proposed frequency-domain approach, an experimental study was carried out. The data acquisition system consists of an arbitrary waveform generator (AWG), a high-speed signal digitizer (DIG), a low noise preamplifier (LNP) and a multiplexer. A pitch-catch test was performed using a pair of PZT (actuator-sensor) patches attached to a specimen. Using the 16-bits AWG, a tone-burst signal with a ± 10 peak-to-peak voltage was generated, and a driving frequency to the excitation PZT patch was varied from 100 kHz to 200 kHz with an increment of 1 kHz. Then, the PZT patch generated elastic Lamb waves on the specimen, and the response was measured at the other sensing PZT patch. The measured voltage output was amplified by the LNP with a gain of 20 and measured by the 14-bits DIG. In order to improve the signal-to-noise ratio, the pitch-catch signals were measured 10 times and averaged in the time-domain. An aluminum plate with a dimension of 610x400x6 mm^3 was tested in this study. Four identical PSI-5AE type PZT patches (10x10x0.508 mm^3) were mounted on both sides of the specimen. PZTs A and D were collocated and attached on the opposite sides of the plate and PZTs B and C were mounted in a similar manner. The arrows denote the positive polling direction of each PZT patch. An intact case (without a notch) and four different damage cases with varying notch locations, orientations and numbers were investigated sequentially.

A.4.1. Undamaged Case

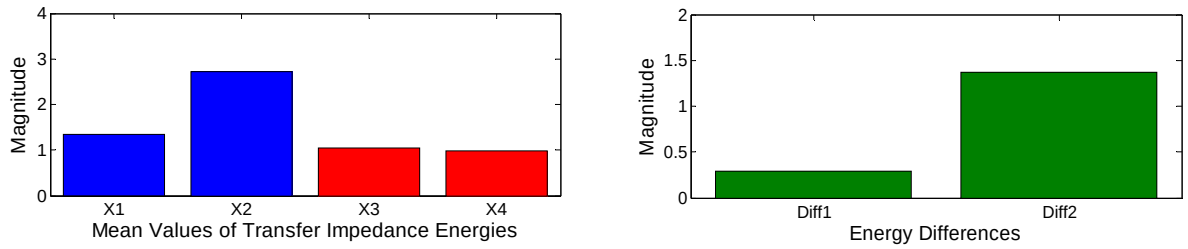

(b) (c)

FIG. 4. Instantaneous damage diagnosis using the averaged transfer impedance energies of signals M1-M4 obtained from the intact condition: (a) transfer impedances of signals M1-M4 obtained from the intact condition of the plate, (b) averaged transfer impedance energies (X1,X2, X3 and X4) of signals M1-M4, and (c) since Diff 1< Diff 2, the plate is diagnosed as in its pristine condition.

First, initial data were collected from the pristine condition of the specimen by varying the driving frequency from 100 kHz to 200 kHz with an increment of 1 kHz. Then, the composition of signals M1-M4 was carried out. As mentioned earlier, ideally they should be zero for the entire length of the signals in the absence of damage. However, due to the PZT imperfections or measurement noises, some initial errors are observed in these signals. Then, the transfer impedances were obtained by taking FFT of signals M1-M4 while sweeping the driving frequency from 100

kHz to 200 kHz with an increment of 1 kHz. Then, the transfer impedance energies of the composed signals (M1-M4) were averaged over the entire frequency band in Fig. 4 (b). Then, the minimum of out-of-class differences (Diff1) and the maximum of within-class differences (Diff2) were computed in Fig. 4 (c). Since 'Diff 1' is smaller than 'Diff 2', it can be stated that the plate does not have a crack that produces mode conversion beyond initial errors and the condition of the specimen can be instantaneously diagnosed as "Healthy Condition". Next, four different damage cases shown in Fig. 5 have been investigated (Damage Case I: crack along direct wave propagation path; Damage Case II: crack behind one of the PZTs; Damage Case III: crack out of direct wave path; and Damage Case IV: multiple cracks).

A.4.2. Damage Case I: crack along the direct wave propagation path

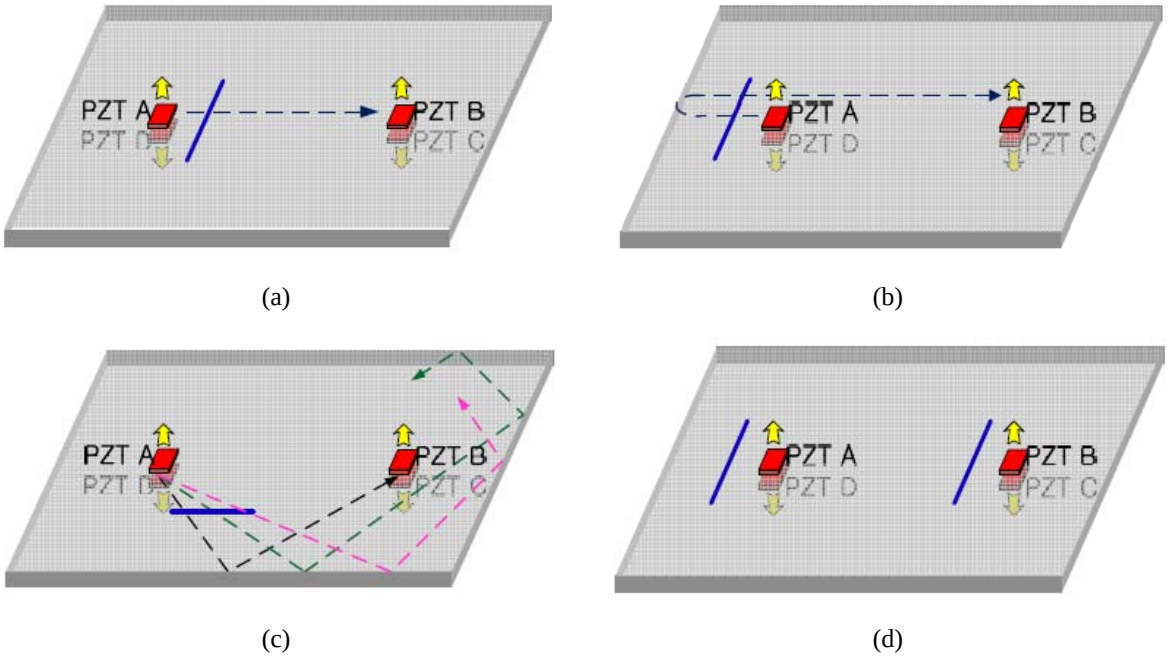

FIG. 5. Four different damage cases investigated in this study: (a) Damage Case I, (b) Damage Case II, (c) Damage Case III, and (d) Damage Case IV (In figures (c) and (d), time signals are omitted because each mode conversions and reflections are complicated to identify in the time-domain).

For Damage Case I shown in Fig. 5(a), a crack with 40 mm in length, 1 mm in width, and 3 mm in depth was introduced along the direct guided wave propagation path between PZTs A and B and closer to PZT A (60 mm apart from PZT A). It is expected that two converted modes, MC_1 and MC_2 due to the crack damage may occur between the fundamental modes, S_0 and A_0 in the forwarding signal AB. Here, MC_1 denotes the S_0/ A_0 mode and the MC_2 does the A_0/ S_0 mode, since the crack is closer to PZT A and the S_0 mode travels faster than the A_0 mode. The signals M1-M4 are obtained at an excitation frequency of 180 kHz and compared with the ones from the intact case. As expected, the appearance of two converted modes (MC_1 and MC_2) are clearly shown between the arrival times of the S_0 and A_0 modes in signals M1 and M2, while only either MC_1 or MC_2 appears in signals M3 and M 4 within the same time segment. However, it should be noted that there are additional converted modes in the reflected regions of all signals and it is difficult to identify each of them.

Fig. 6(a) shows the corresponding transfer-impedances of signals M1-M4. Then, the average energies for transfer impedances were computed in Fig. 6(b), and instantaneous damage diagnosis was subsequently performed on them as displayed in Fig. 6(c). It should be noted that the overall energy level of Damage Case I shown in Fig. 6(b) is much higher than that of the intact case shown in Fig. 4(b). Furthermore, it is observed that the energy ratio of Class A transfer impedances to Class B impedances tends to be close to 2:1. Since 'Diff 1' is larger than 'Diff 2' in Fig. 6 (c), the presence of damage is instantaneously identified.

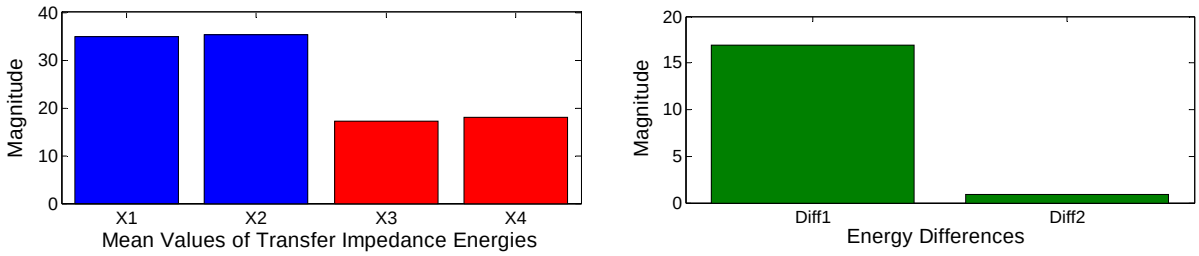

(b) (c)

FIG. 6. Instantaneous damage diagnosis using the averaged transfer impedance energies of signals M1-M4 obtained from Damage Case I: (a) transfer impedances of signals M1-M4 obtained from Damage Case I of the plate, (b) averaged transfer impedance energies (X1,X2, X3 and X4) of signals M1-M4, and (c) since Diff 1> Diff 2, the plate is diagnosed as in its damaged condition.

A.4.3 Damage Case II: crack behind one of the PZTs

In this subsection, Damage Case II shown in Fig. 5(b) has been investigated. A crack of the same size (40x1x3 mm^3) as the previous example was introduced 60 mm behind PZT A. Then, converted modes, MC_1 and MC_2 would appear as part of signals reflected from one of the boundaries close to PZT A rather than as part of direct path signals between the first arrivals of the S_0 and A_0 modes. The same procedure was repeated for the composition of M1-M4, calculation of transfer impedances, and damage classification. The average energies of the proposed transfer impedances were computed in Fig. 7(a), and instantaneous damage diagnosis was performed as in Fig. 7(b). It is observed that the energy ratio tends to be near "2:1" between Class A transfer impedances (for the first two) and Class B impedances (for the last two). Subsequently, the condition of the specimen has been instantaneously diagnosed as "Damaged Condition", since 'Diff 1' is larger than 'Diff 2'. Note that the proposed frequency-domain approach provides robust crack diagnosis even when the converted modes appear as part of the reflected signals.

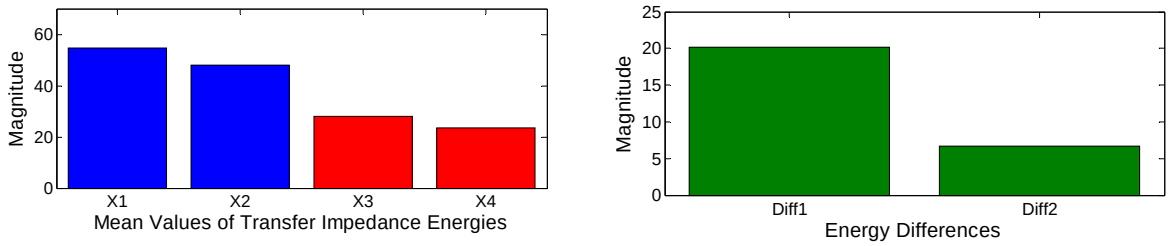

(a) (b)

FIG. 7. Instantaneous damage diagnosis using the averaged transfer impedance energies of signals M1-M4 obtained from Damage Case II: (a) averaged transfer impedance energies (X1,X2, X3 and X4) of signals M1-M4 and (b) since Diff 1> Diff 2, the plate is diagnosed as in its damaged condition.

A.4.4. Damage Case III: crack out of the direct wave path (side)

As the third damage case, a crack of the same size as before was introduced between PZTs A and B but off the direct wave path, as shown in Fig. 5(c). Here, the crack is carefully oriented and positioned so that the converted modes need to be reflected from the boundaries several times before they can measured at PZT B. The same procedures were repeated for the composition of M1-M4, calculation of transfer impedances, and damage classification. It is noted that the identification of both mode conversions and fundamental modes becomes challenging in the time-domain. The average energies of the transfer impedances were computed in Fig. 8(a), and instantaneous damage diagnosis was shown in Fig. 8(b). Again, it is observed that the energy ratio tends to be near

"2:1" between Class A (for the first two) and Class B (for the last two). The results in Fig. 8 indicate that the condition of the specimen has been instantaneously diagnosed as "Damaged Condition", since 'Diff 1' is larger than 'Diff 2'. It is, therefore, confirmed that the proposed frequency-domain approach provides robust crack detection results regardless of crack locations and orientations.

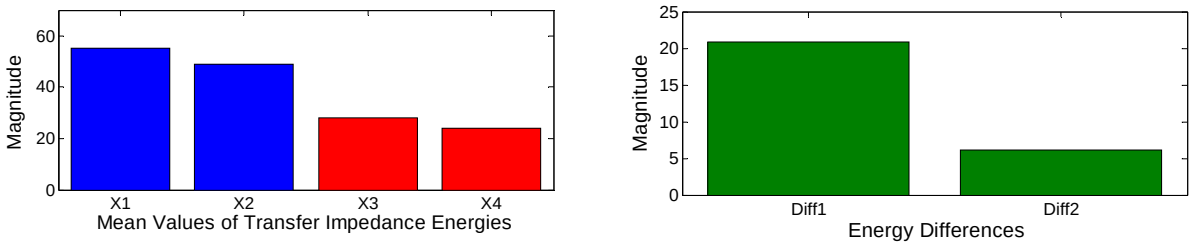

(a) (b)

FIG. 8. Instantaneous damage diagnosis using the averaged transfer impedance energies of signals M1-M4 obtained from Damage Case III: (a) averaged transfer impedance energies (X1,X2, X3 and X4) of signals M1-M4 and (b) since Diff 1> Diff 2, the plate is diagnosed as in its damaged condition.

A.4.5. Damage Case IV: multiple cracks

As the final damage case, two cracks of the same size of 40x1x3 mm^3 were introduced along and out of the direct wave path, as shown in Fig. 5(d). It can be expected that multiple mode conversions occur not only when Lamb waves propagate along the direct path but also when reflected from boundaries. The average energies for the transfer impedances were computed in Fig. 9(a) and instantaneous damage diagnosis result was subsequently reported in Fig. 9(b). All the results in Fig. 9 were consistent with the ones from the previous damage cases. Furthermore, the magnitudes of the averaged transfer impedance energies for Damage Cases IV (Fig. 9) were larger than those from the previous Damage Cases I-III (Figs 9, 10 and 11). It can be, therefore, confirmed that the proposed reference-free damage detection technique works well even in the presence of multiple cracks regardless of the crack locations and orientations.

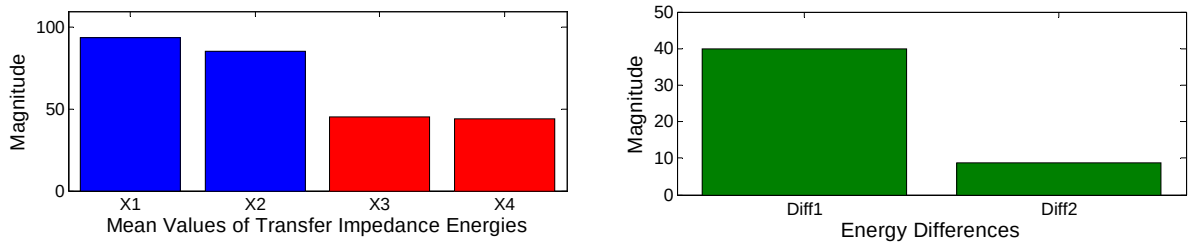

(a) (b)

FIG. 9. Instantaneous damage diagnosis using the averaged transfer impedance energies of signals M1-M4 obtained from Damage Case IV: (a) averaged transfer impedance energies (X1,X2, X3 and X4) of signals M1-M4 and (b) since Diff 1> Diff 2, the plate is diagnosed as in its damaged condition.

B. Instantaneous crack detection under varying temperature and static loading conditions

B.1. Introduction

In this study, first, the reference-free technique is reformulated considering energy distributions among Lamb wave modes to overcome the limitations of the previous time domain approach. Second, the data acquisition time has been significantly reduced by allowing the use of various input waveforms such as narrowband toneburst signals and broadband chirp signals. Finally, the robustness of the improved reference-free technique to varying temperature and external loading has been experimentally validated.

B.2. Theoretical development

B.2.1. Development of a dual-PZT

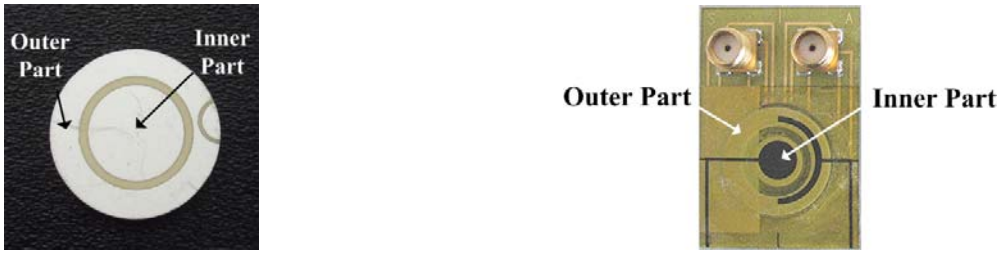

(a) (b)

FIG. 10. Design of dual-PZT transducers: (a) Raw dual-PZT and (b) Packed dual-PZT

The previous reference-free technique isolated the mode conversion produced by crack formation using two pairs of collocated PZT transducers. Here, it was necessary to collocate two identical PZT transducers on top and bottom surfaces of the structure. However, often access to both surfaces of a structure can be limited, and it can be difficult to precisely place two PZTs at the same position but on the opposite sides. To overcome this limitation, a new PZT design coined "dual-PZT" is developed as shown in Fig. 10(a). The dual-PZT is divided into inner circle and outer ring parts. These segmentations of the dual-PZT allow excitation and sensing of guided waves using the inner circle, the outer ring or the both parts simultaneously. It will be shown in the next subsection how this selective guided wave actuation and sensing using different PZT sizes can be applied to the isolation of mode conversion signals induced by a crack.

For field deployments, the ruggedness of the PZT transducer is critical because the PZT transducer itself can be the weakest link in the entire SHM system. In this study, a new packed dual-PZT shown in Fig. 10(b) is developed so that the bare PZT can be encapsulated using a Kapton tape with printed circuits. This packed PZT design makes the PZT installation easier, achieves a reliable wire connection and insulates the ground of the PZT transducer from the host structure, minimizing electromagnetic interference.

Next, the notations used to describe the time signals measured from a pair of dual-PZTs are introduced. 'F' denotes a forward signal excited by a left PZT (PZT A) and measured by the other PZT (PZT B) on the right side. 'B' represents a backward signal propagating in the opposite direction. The subscripts '1', '2' and '3' represent the entire area, the outer ring part and the inner circle part of a dual-PZT, respectively. The darker (red) area of a PZT denotes the PZT area activated for PZT excitation or sensing. For example, F_{31} represents the forward signal excited by the inner circle part of PZT A and measured by the whole area of PZT B.

B.2.2. Extraction of mode conversion

Lamb waves can propagate in two types of modes, symmetric (S) and anti-symmetric (A) modes. When Lamb waves propagating along a plate-like structure encounter a sudden thickness change such as a crack on the structure, portion of a Lamb wave mode is transformed into the other mode. This phenomenon is defined as mode conversion. For example, when a S_0 mode passes through a crack, part of the transmitted S_0 mode is converted into an A_0 mode (A_0/ S_0) and the rest remain unchanged (S_0/ S_0). Similarly, S_0/ A_0 and A_0/ A_0 are defined.

Here, it is explained how converted Lamb wave signals can be extraction from the various signals measured by a pair of dual-PZTs. The basic premise is that, when PZTs with different sizes are used for measuring F_{ij} and B_{ij} ($i \neq j$), converted modes (A_0/S_0 and S_0/A_0) appear in D_{ij} ($= F_{ij} - B_{ij}$) only when damage exists. For example, Fig. 11(a) shows that F_{13} and B_{13} are identical in the time domain when there is no damage. Therefore, the difference D_{13} ($=F_{13} - B_{13}$) becomes a null signal. On the other hand, converted modes, A_0/S_0 and S_0/A_0, appear in F_{13} and B_{13} of Fig. 11(b) when

crack is formed. Here, A_0/S_0 in F_{ij} is identical to S_0/A_0 in B_{ij} (not to A_0/S_0 in B_{ij}), and S_0/A_0 in F_{ij} is reciprocal to A_0/S_0 in B_{ij}. Note that A_0/S_0 in F_{ij} exactly matches with A_0/S_0 in B_{ij} only when the size of the exciting PZT is same as that of the sensing PZT (i=j). Therefore, converted modes can be isolated by subtracting B_{ij} from F_{ij}, and the extracted mode conversion appears in D_{ij}. Here, a total of 6 different D_{ij} signals can be constructed from 6 different pairs of i and j. Note that signals F_{ij} and B_{ij} are defined as pair signals in this study. The subsequent damage classifier will be built on these extracted mode conversion signals.

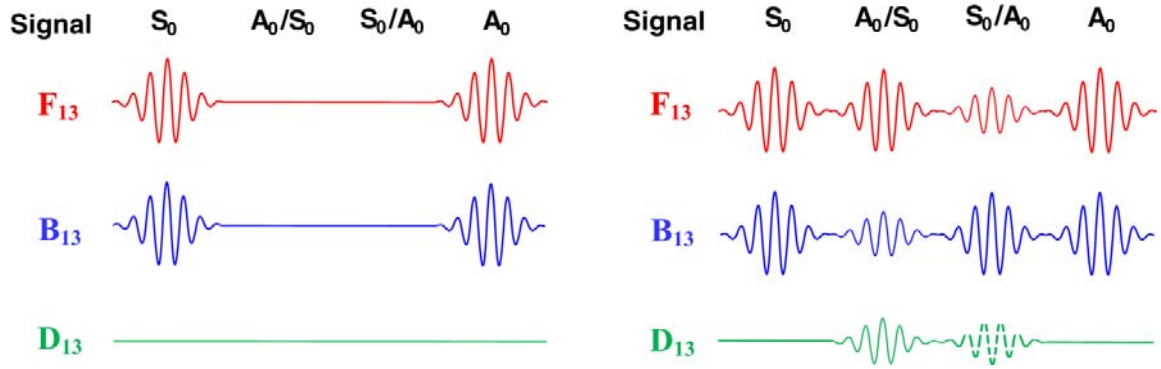

(a) (b)

FIG. 11. Extraction of mode conversion in the time domain: (a) There is no difference between F_{13} and B_{13} signals without damage, and (b) Mode conversion appears in signal D_{13} ($=F_{13} - B_{13}$) with damage.

B.2.3. Superposition relationships among measured signals

Here, superposition relationships among measured signals are exploited to establish the necessary threshold value for the damage classification introduced in the next subsection. The first superposition relationship is concerned with the variation of the exciting PZT size. It shows the summation of the response signals obtained by the outer ring excitation (F_{2j}) and the inner circle actuation (F_{3j}) is equal to the response corresponding to the whole area PZT excitation (F_{1j}) for any fixed sensing PZT size, j.

$$F_{1j} = F_{2j} + F_{3j} \qquad \text{for} \quad j = 1 \sim 3 \tag{B.1}$$

Next, the other superposition relationship for varying sensing PZT size is established. In terms of sensing, the output voltage of a sensing PZT is proportional to the size of the PZT. Consequently, the response signal measured by the whole PZT area becomes identical to the weight sum of the responses obtained by the outer ring and the inner circle parts regardless of the size of the exciting PZT.

$$F_{i1} = \alpha F_{i2} + \beta F_{i3} \qquad \text{for} \quad i = 1 \sim 3 \tag{B.2}$$

where $\alpha + \beta = 1$, and α and β values are the ratios of the outer and inner PZT sizes to the whole PZT size, respectively. For instance, if the sizes of the outer and inner parts are identical, both α and β become 0.5. Note that all superposition relationships described here are also valid for backward signals and regardless of the presence of damage.

B.2.4. Reference-free damage classification

In this subsection, a reference-free damage classifier that operates on the extracted mode conversion signals is developed. First, the energy level of the crack-induced mode conversion is computed by transferring the mode conversion signals in the time domain into the frequency domain. Second, a threshold value is calculated from the energy level of the error signals that stem from the imperfect matching of the aforementioned superposition

relationships. Finally, when the energy level of the mode conversion exceeds the error energy level, the structure is adjudged damaged.

First, the mode conversion energy (MCE) is computed from the mode conversion time signals: (1) The mode conversion time signal D_{ij} (= F_{ij} - B_{ij}) is extracted at a specific driving frequency; (2) D_{ij} is converted to the frequency domain using the Fast Fourier Transform (FFT); (3) The previous two steps are repeated over the entire frequency range of interest; (4) MCE is defined as the summation of the magnitude of D_{ij} in the frequency domain over the entire frequency range.

$$MCE_{ij} = \frac{2E(D_{ij})}{E(F_{ij}) + E(B_{ij})} \quad \text{for } i \neq j \tag{B.3}$$

where $E(D_{ij})$ denotes the FFT of D_{ij} over the entire frequency range investigated ($E(D_{ij}) = \int FFT(D_{ij})df$). Note that the mode conversion energy is normalized by the energy levels of F_{ij} and B_{ij}, and a total of 6 MCE values can be obtained. Finally the averaged mode conversion energy (AMCE) is defined as the average of these 6 MCE values and this value is used for the subsequent damage classification.

Second, the normalized energy levels of the errors inherent in the superposition relationships are computed in a manner similar to the computation of MCE.

$$FAE_{1j} = \frac{2E(F_{1j} - F_{2j} - F_{3j})}{E(F_{1j}) + E(F_{2j} + F_{3j})} \quad \text{for } j = 1 \sim 3 \tag{B.4}$$

$$FSE_{1j} = \frac{2E(F_{i1} - \alpha F_{i2} - \beta F_{i3})}{E(F_{i1}) + E(\alpha F_{i2} + \beta F_{i3})} \quad \text{for } j = 1 \sim 3 \tag{B.5}$$

where the first 3 error energy levels, FAE_{1j}, are computed from the excitation superposition relationships of F_{ij} signals, and the last 3 are from the sensing superposition relationships. Additional 6 error energy levels can be also computed from B_{ij} signals, producing a total of 12 error energy levels.

Finally, an instantaneous reference-free damage classifier is established. The threshold value is established from the previously computed 12 error energy levels using extreme value statistics. First, a Weibull distribution is fit to the error energy levels, and the threshold is set in accordance to a one-sided 95.4% confidence interval. Damage is alarmed when AMCE exceeds the threshold value. Otherwise, the structure is diagnosed undamaged.

B.3. Numerical simulation

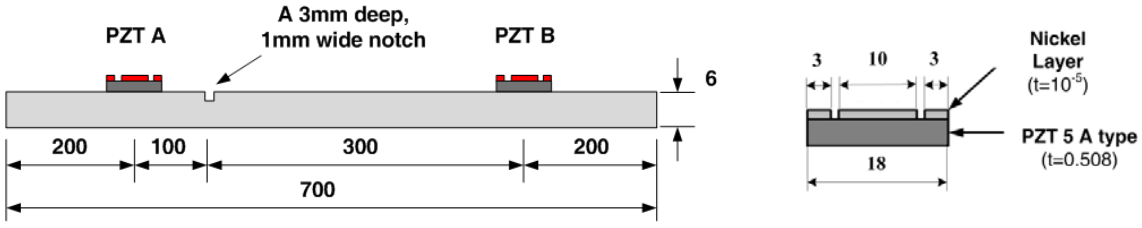

(a) (b)

FIG. 12. Numerical simulation setup: (a) specimen and (b) dual-PZT transducer (All dimensions are in mm)

The proposed technique for crack detection was first validated through 2-D numerical simulations, using the plain strain assumption. The simulations were performed using COMSOL 3.3a Multi-physics software with the mapped mesh (1mm x 1mm maximum size), the sampling rate of 4 MS/sec, the mass damping coefficient of 10^{-4}, the absolute tolerance of 10^{-11} and the second order Max. BDF. An aluminum plate, that is 70 cm long and 6 mm thick, is used for numerical simulation. For the damaged case, a 3 mm deep and 1mm wide notch was introduced 100 mm

away from PZT A as shown in Fig. 12(a). Two identical dual-PZTs were placed on the top surface of the plate as shown in Fig. 12(b). PSI-5AE type PZTs were used for the simulations. Here, the thickness and the diameters of the inner and outer PZTs were 0.508 mm, 10 mm and 18 mm, respectively. A narrowband toneburst signal at 150 kHz was used as an input signal.

B.3.1. Extraction of mode conversions in the time domain

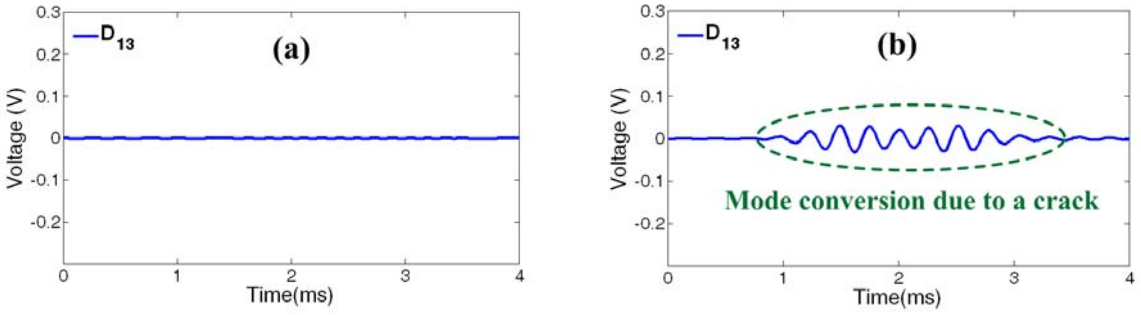

(a) (b)

FIG. 13. Extraction of mode conversion signal D_{13} (=F_{13}-B_{13}) obtained from simulation at 150 kHz: (a) Intact case and (b) Damaged case

Fig. 13(a) shows that no mode conversion appears in D_{13} (=F_{13}-B_{13}) when F_{13} and B_{13} were obtained from the intact condition of the plate. On the other hand, the mode conversion clearly appeared when the notch was introduced. Similar results were obtained as long as different PZT sizes were used for excitation and sensing.

B.3.2. Superposition relationships among measured signals in the time domain

Here, the superposition relationships described in Equations (B.1) and (B.2) were verified through numerical simulations. Figs 14(a) and (b) show the superposition relationships with varying exciting and sensing PZT sizes obtained from the intact condition, respectively. Note that α and β coefficients were calculated to be 0.643 and 0.357, respectively, based on the PZT dimensions. These superposition relations were also verified for different PZT pairs and the damage case although they were not reported here due to the space limit.

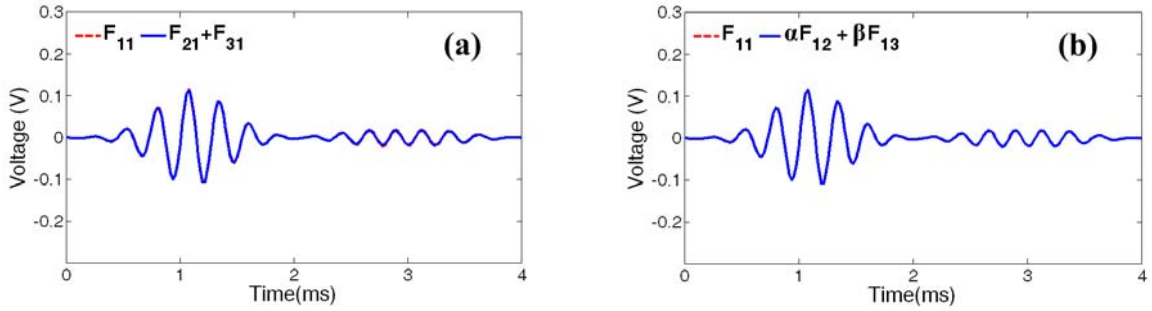

(a) (b)

FIG. 14. Numerical verification of the superposition relationships described in Equations (B.1) and (B.2): (a) Varying exciting PZT sizes $(F_{11} = F_{21} + F_{31})$ and (b) Varying sensing PZT sizes ($F_{11} = \alpha F_{12} + \beta F_{13}$)

B.4. Experimental verification

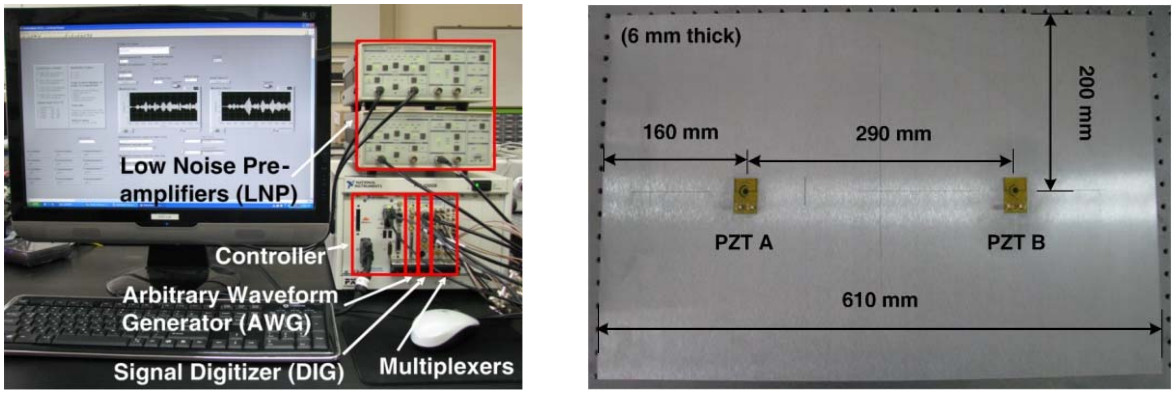

FIG. 15. Experimental setup and test specimen

Next, the effectiveness of the proposed reference-free crack detection technique was examined through laboratory experiments conducted on aluminum plates with the dimensions of 610 mm x 400 mm x 6 mm. The overall test setup and the test specimen are shown in Fig. 15. The data acquisition system consisted of an arbitrary waveform generator (AWG), a high-speed signal digitizer (DIG), a low noise preamplifier (LNP) and multiplexers. Using the 16-bits AWG, toneburst and chirp input signals with a $\pm$ 10 peak-to-peak voltage were generated. In order to compute the mode conversion and error energies, a driving frequency range of 100 kHz to 150 kHz with 10 kHz increment was used for both the toneburst and chirp input signals. The output voltage was measured by the 14-bits DIG. Then, the response signals were measured 10 times and averaged in the time-domain to improve the signal-to-noise ratio. Also, a bandpass filter with 1 kHz and 1 MHz cutoff frequencies was used.

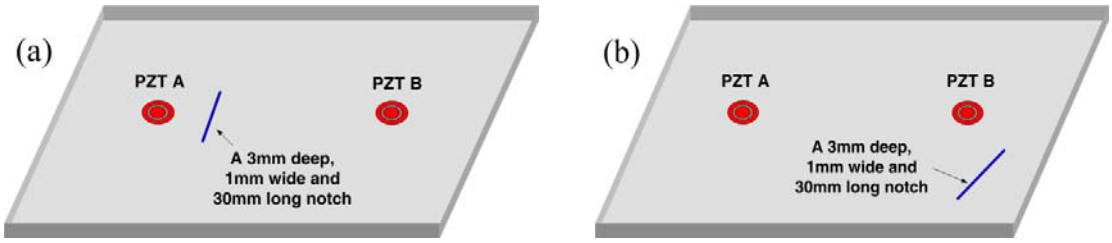

(a) (b)

FIG. 16. Experimentally investigated damaged cases: (a) Damage case I and (b) Damage case II

Newly designed dual-PZT patches described in Fig. 10(b) were mounted on one side of the specimen as shown in Fig. 16. The thickness and the diameters of the inner and outer PZTs were 0.508mm, 8 mm and 18 mm, respectively. Investigated damage cases are shown in Fig. 16. In damage case I, a notch was introduced between PZTs A and B, but a notch was placed out of the direct wave propagation path for damage case II.

B.4.1. Instantaneous damage classification

First, the damage classification was performed on the AMCE values obtained using toneburst input signals. Fig. 17 shows that the threshold value was greater than AMCE for the intact case. Then, the AMCE value exceeded the threshold value for all the subsequent damage cases. Similar results were observed when chirp input signals were used instead of the toneburst signals as reported in Fig. 18. When toneburst input singles were used, the data collection time increased proportionally to the number of the driving frequencies investigated. On the other hand, the chirp input signals reduced the data collection time significantly without compromising damage diagnosis.

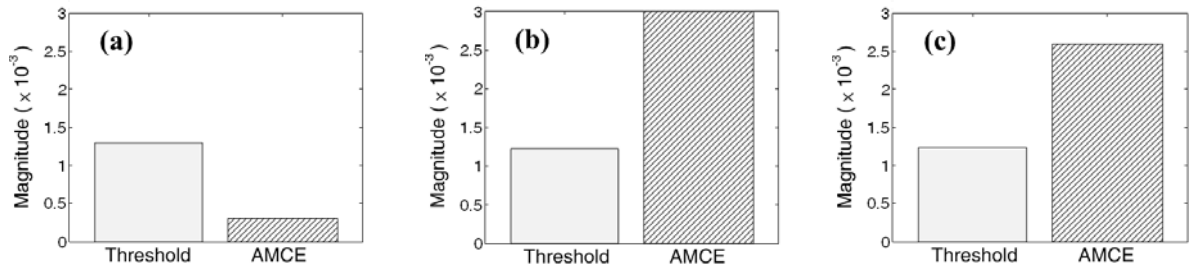

FIG. 17. Reference-free damage classification using toneburst input waveforms: (a) Intact case, (b) Damage case I and (c) Damage case II (Note that Threshold and AMCE denote the instantaneous threshold value obtained from error energy and the averaged mode conversion energy, respectively. The structure is adjudged damaged when AMCE exceeds Threshold.)

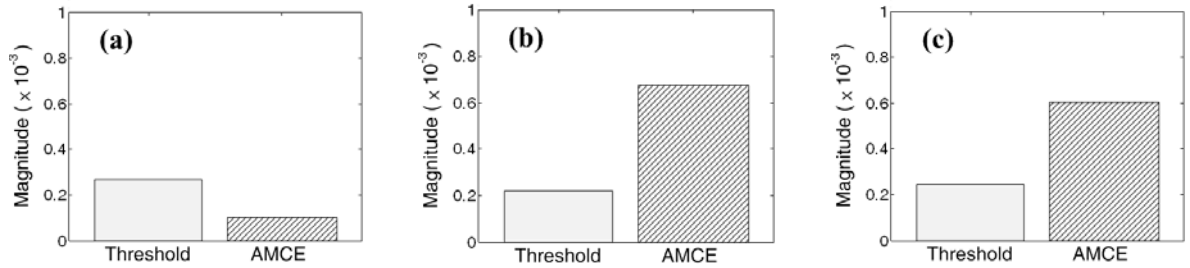

FIG. 18. Reference-free damage classification using chirp input waveforms: (a) Intact case, (b) Damage case I and (c) Damage case II (Note that Threshold and AMCE denote the instantaneous threshold value obtained from error energy and the averaged mode conversion energy, respectively. The structure is adjudged damaged when AMCE exceeds Threshold.)

B.4.2. The effect of temperature and static loading variations

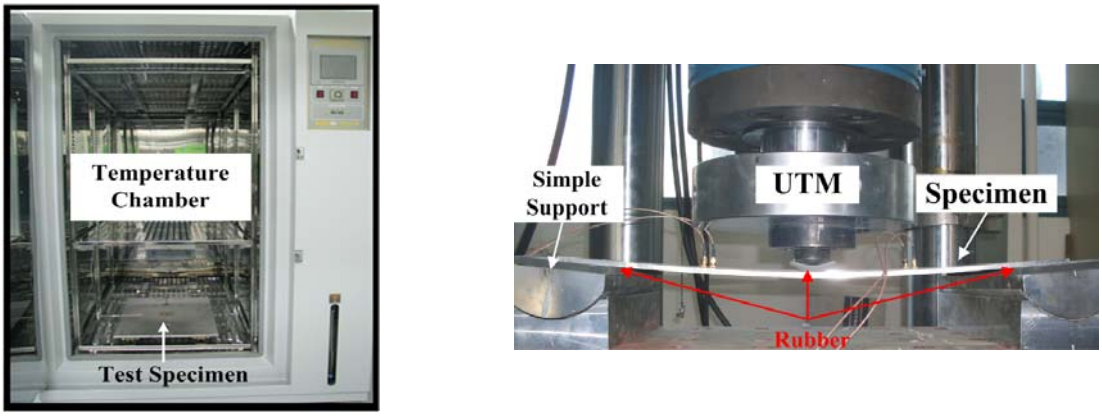

(a) (b)

FIG. 19. Experimental setups for temperature and loading tests: (a) Temperature chamber and (b) Universal Test Machine (UTM)

Here, the robustness of the proposed technique under changing temperature and loading conditions is investigated. Fig. 19 shows the temperature chamber and universal test machine (UTM) used in this study. All the other experimental setups and the investigated damage cases are same as the previous ones unless noted differently.

The temperature chamber can control both temperature and humidity. For the temperature experiment presented in this study, damage diagnosis was conducted at -30°C, 0°C, 20°C and 50°C with 30% humidity above 0°C. Also, a thermocouple was used to measure the temperature of the specimen's surface within the temperature chamber.

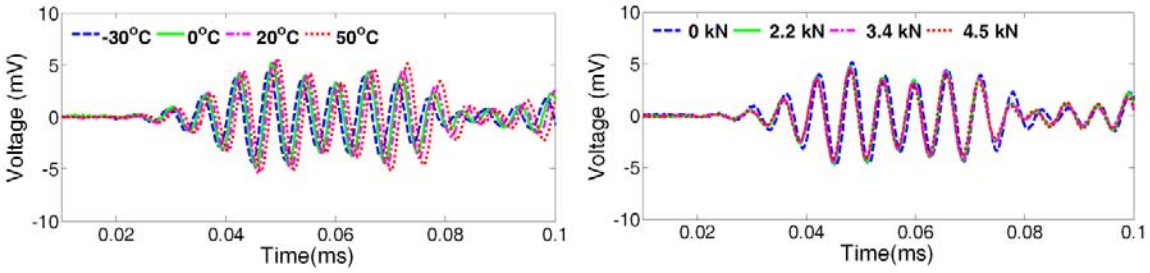

(a) (b)

FIG. 20. Variations of mode conversion signal D_{13} under changing temperature and loading conditions: (a) Under varying temperature and (b) Under varying loading levels

Fig. 20(a) shows the mode conversion signal D_{13}, obtained from different temperature conditions of damage case I. Although the mode conversion appears at all temperatures, the phase and amplitude of the mode conversion signal changed. In spite of these temperature-induced variations of the time signals, Table I shows that the proposed damage classifier correctly detected the two damage cases under varying temperature.

Next, damage diagnosis was repeated under varying loading conditions. A simple three-point loading test as shown in Fig. 19(b) was performed under displacement control. To avoid the direct contact of the specimen with the UTM tip and the iron supports, rubber pads were inserted at these contact surfaces. Lamb wave signals were collected when the midpoint displacement of the specimen was 10mm, 15mm and 20mm, respectively.

The loading forces corresponding to these displacements were calculated to be 2.2kN, 3.4kN and 4.5kN, respectively, considering the material properties, shape and boundary conditions of the specimen. Amplitude and velocity variations of the mode conversion signal were observed in Fig. 19(b), and similar results were reported in the literature. Similar to the temperature experiments, satisfactory damage classification results are reported in Table I for the varying loading cases. In this study, the loading was controlled so that the maximum strain within the specimen would stay within an elastic range. In practice, excessive strain can lead to the performance deterioration of the PZTs and even cause PZT defects.

4. Summary and Conclusion

In this project, the applicability of the proposed damage diagnosis techniques to crack detection has been fully validated throughout numerical as well as experimental studies. Summaries and conclusions of the proposed approaches are as follow:

Reference-free crack detection using transducer impedance: A reference-free crack detection technique has been developed for plate structures so that crack formation could be identified using transfer impedances between pitching and catching PZTs. This transfer impedance technique advances the previously developed time-domain technique so that mode conversion produced by a crack formation can be detected in the frequency-domain rather than in the time-domain. In the previous time-domain approach, individual Lamb wave modes such as S_0, A_0 and converted modes should be decomposed and identified in the time-domain. However, these procedures can be complicated when the crack is not directly along the wave path and there are multiple reflections and additional higher modes. Furthermore, extra caution is required to determine several design parameters during experiments. For instance, an optimal driving frequency needs to be selected after examining a Lamb wave tuning curve and the truncation time point should be carefully decided for signal collection. On the other hand, the proposed frequency-domain approach does not require the selection of a single optimal driving frequency or the decomposition of individual Lamb modes, since it only considers the crack-induced energy increase over some frequency range. Furthermore, since only the overall energy

increase produced by mode conversion is concerned, the proposed technique is less responsive to the driving frequency range and the length of each time signal. Another advantage of this study is that not only a single crack but also multiple cracks can be detected even when the crack(s) is (are) not along a direct wave path.

Instantaneous crack detection under varying temperature and static loading conditions: A new reference-free crack detection technique that utilizes specially designed PZTs placed on a single surface of a structure to detect crack damage in a plate-like structure is developed. The basic premise of the proposed technique is that the mode conversion induced by a crack can be extracted from various signal pairs measured by the newly designed PZTs, and the mode conversion exceeding an instantaneously established threshold can be detected by exploiting the superposition relationships among measured signals. The proposed technique can detect cracks even when measured Lamb wave time signals are complex due to the existence of multiple modes and reflections, overcoming the limitation of the previous reference-free techniques in the time domain. Moreover, the data collection time has been significantly reduced by allowing the use of broadband chirp input waveforms as well as narrowband tonebust signals. The instantaneous threshold for damage classification is established using the signals acquired only from the current condition of the structure. Finally, the robustness of the proposed technique against not only temperature changes but also varying external static loading is verified.

5. Reference

1. Raghavan, A., Cesnik, C.E.S. Review of guided-wave structural health monitoring. *Shock and Vibration Digest* 2007; **39**(2): 91-114.
2. Rose, J. A Baseline and Vision of Ultrasonic Guided Wave Inspection Potential. *Journal of Pressure Vessel Technology, Transactions of the ASME* 2002; **124**(3): 273-282.
3. Ihn, J.B., Chang, F.K. Detection and monitoring of hidden fatigue crack growth using a built-in piezoelectric sensor/actuator network: I. Diagnostics. *Smart Materials and Structures* 2004; **13**(3): 609-620.
4. Sohn, H. Effects of Environmental and Operational Variability on Structural Health Monitoring. *Philosophical transactions of the Royal Society A* 2007; **365**(1851): 539-560.
5. Kim, S. B., Sohn, H. Instantaneous reference-free crack detection based on polarization characteristics of piezoelectric materials. *Smart Materials and Structures* 2007; **16**(6): 2375-2387.
6. Kim, S. B., Sohn, H. Instantaneous Crack Detection using Dual-PZT Transducers. *Proceedings of SPIE-The International Society for Optic Engineering* 2008; 693509.
7. Viktorov, I. Rayleigh and Lamb Waves. *Plenum Press* 1967; New York.
8. Cho, Y. Estimation of Ultrasonic Guided Wave Mode Conversion in a Plate with Thickness Variation. *IEEE Transactions on Ultrasonics, Ferroelectrics and Frequency Control* 2000; **47**(3): 591-603.
9. Raghavan, A., Cesnik, C.E.S. Finite-dimensional piezoelectric transducer modeling for guided wave based structural health monitoring. *Smart Materials and Structures* 2005; **14**(6): 1448-1461.
10. Sohn, H., Lee, S.J. Lamb Wave Tuning Curve Calibration for Surface-bonded PZT Transducers. *Smart Materials and Structures* 2010; **19**(1): 015007.
11. Park, H.W., Sohn, H. Parameter Estimation of the Generalized Extreme Value Distribution for Structural Health Monitoring. *Journal of Probabilistic Engineering Mechanics* 2006; **21**(4): 366-376.